Lipopolymer electrophoresis in supported bilayer membranes

Huai-Ying Zhang and Reghan J. Hill*

Received 13th June 2010, Accepted 6th August 2010
DOI: 10.1039/c0sm00524j

We report theory and experiments investigating the electric-field-induced drift of poly(ethylene glycol) (PEG)-derivatized lipids in supported lipid bilayer (SLB) membranes. Based on classical continuum models, an analytical formula for the lipopolymer electrophoretic mobility is derived, drawing upon the Debye–Hückel approximation. The model is extended to the high membrane surface charge densities encountered in experiments by drawing upon the Guoy-Chapman theory to correct the surface charge-surface potential relationship. This convenient approximation is successfully tested by comparison with numerical solutions of the electrokinetic model based on the non-linear Poisson–Boltzmann equation. We use the analytical model to interpret measured electrophoretic mobilities of 1,2-distearoyl-sn-glycero-3-phosphoethanolamine-N-[poly(ethylene glycol)2000-N′-carboxyfluorescein] (DSPE-PEG2k-CF) in glass-supported 1,2-dioleoyl-sn-glycero-3-phosphocholine (DOPC) bilayers at DSPE-PEG2k-CF concentrations up to 5 mol%. By separating the frictional force on lipopolymers into separate lipid-tail and polymer-chain contributions, experimental trends are captured. Fitting the model to the data furnishes several previously unknown model parameters, namely the hydrodynamic size of a polymer segment, and a polymer-bilayer frictional coupling coefficient. We show that electro-osmotic flow plays a determinative role in the lipopolymer drift. For DSPE-PEG2k-CF in DOPC, electro-osmotic flow yields significantly lower electrophoretic mobilities than expected by balancing the total lipopolymer electrical force with the Stokes–Einstein frictional force. This is attributed to the hydrodynamic coupling of PEG chains to the oppositely directed electro-osmotic flow.

Jaffe[1] first proposed lateral electrophoresis in cell membranes as a possible cellular organization mechanism. At about the same time, Poo and Robinson[2] reported the redistribution of protein concanavalin-A receptors along embryonic muscle cells in an external electrical field. Since then, electrical migration of many cell surface receptors and membrane proteins—in a variety of cell types—has been observed experimentally. Theoretical interpretation of the electrokinetic phenomena, however, has been hindered by the complexity of native cell membranes[3–6] Recent advances in solid supported lipid bilayers (SLBs) as model cell surfaces have enabled elaborate quantitative analysis of the effects of electric fields on membrane organization.[7–9] Extensive investigations of the electrophoretic motion of lipids and proteins within SLBs have therefore been undertaken.[10–13] SLBs containing lipopolymers furnish a powerful model system to advance our understanding of cell membrane dynamics. Control over the polymer grafting density, layer thickness, and surface charge density can be achieved,[14] and transmembrane proteins can be integrated into SLBs with lipopolymers acting as a spacer to eliminate the bilayer-substrate interaction and, thus, maintain protein mobility. Accordingly, lipopolymers in model membranes have been proposed to mimic glycocalyx.[15]

SLBs containing lipopolymers are promising in biotechnology, due, in part, to their fluid and air stability.[16] Moreover, lipopolymer conformation can be tuned by varying the surface concentration, imparting control over ligand-receptor binding.[17,18] Electrophoresis in SLBs has been demonstrated to be sensitive enough to separate isomers of Texas red.[19] Moreover, a "spatially resolved label-free" analysis of composition gradients in SLBs has been achieved by electrophoretic manipulation in concert with surface micro-patterning and laminar flow.[20] Lipopolymer concentration gradients in patterned SLBs using electric fields have potential in biosensing and protein separation applications. Accordingly, detailed studies of the electric-field-induced response may improve the design and quantitative analysis of such diagnostic platforms.

Here we undertake an experimental and theoretical study of the electric-field-induced drift of lipopolymers in SLBs. The lipopolymer in this work has poly(ethylene glycol) (PEG) covalently grafted to a charged phospholipid anchor (DSPE) with the free end bearing a charged fluorescent moiety (carboxyfluorescein) to permit quantitative imaging. In a mean-field approximation, where the charged ends are assumed to be uniformly distributed throughout the polymer layer, the PEG chains resemble a weakly charged polyelectrolyte. In addition to thermodynamic and hydrodynamic interaction forces, the lipopolymers experience an electrical force when subjected to a longitudinal electric field.

Drawing on classical polymer physics, hydrodynamics, and electrokinetic theory, we develop a mathematical model for the electric-field-induced lipopolymer drift. This provides a quantitative interpretation of the experimentally measured lipopolymer electrophoretic mobility $\mu_E = V/E$, defined as the ratio of the polymer drift velocity V to the strength of the longitudinal electric field strength E. Note that V reflects not

Department of Chemical Engineering, McGill University, Montreal, Quebec, H3A 2B2, Canada. E-mail: reghan.hill@mcgill.ca

only the lipopolymer intrinsic charge but also the charge of the host lipids. Moreover the host lipids may present a counter charge that drives electro-osmotic flow outside the bilayer in addition to producing 'hydrodynamic' disturbances within the bilayer.

For example, in bilayers with only 1 mol% charged lipids, each bearing a single elementary charge $-e$, the surface charge density $\sigma \approx -0.25$ μC cm^{-2}, yielding an electrostatic surface potential $\zeta \approx -5.3k_BT/e$ in a very weak electrolyte with Debye screening length $\kappa^{-1} \approx 100$ nm at room temperature. Accordingly, in the absence of lipopolymer, the Helmholtz-Smoluchowski slip velocity driven by an electric field $E = 10$ V cm^{-1} is about 160 μm s^{-1}. Note that bilayer phospholipids attain much lower electro-osmotic velocities, because the lipid head protrudes only a small distance into the electro-osmotic boundary layer, and there is significant frictional drag from the lipid tails within the bilayer itself.[13] For lipopolymers, the polymer hydrodynamic drag makes the electrophoretic mobility much more susceptible to electro-osmotic flow. We seek to capture these and other influences by drawing on tractable continuum approximations of the many-body hydrodynamic, electrostatic, and steric interactions.

1 Theory

Previous studies of SLBs without lipopolymers assumed that the bilayer and support reside on the same plane.[8,9] The glass support was estimated to contribute a surface charge density $\sigma = -0.25$ C m^{-2}, and electrostatic screening in the intervening ~ 1 nm layer of water was neglected. In our experiments, however, the bilayer-support separation is generally considered to be comparable to the ~ 7 nm unperturbed root-mean-squared end-to-end distance of the grafted polymer. Moreover, water trapped between the bilayer and support is thought to maintain the relatively high ionic strength of the electrolyte buffer that is present during bilayer synthesis.[21] Thus, because the ~ 1 nm Debye length is shorter than the ~ 7 nm bilayer-support separation, electrostatic interactions between the bilayer and support may be neglected. Indeed, we assume there are negligible influences of the substrate on the (upper) leaflet.

The obstructed diffusivity of lipids and proteins by absorbed polymers or lipopolymers in one leaflet has been shown to equally hinder dynamics in the other leaflet. It is therefore generally considered that the two leaflets are strongly coupled.[22,23] Such coupling is assumed for electro-migrating lipopolymers, and, accordingly, we interpret our experiments as two strongly coupled leaflets. Thus, while our calculations explicitly address the upper leaflet, coupling with the bottom leaflet is implicitly accounted for through a lipid-tail friction coefficient γ_t. Moreover, we assume lipopolymers maintain a uniform surface mole fraction c while subjected to a longitudinal electric field E. According to Monte Carlo lattice calculations,[24] this is reasonable when $c < 10$ mol%.

The single negative charge of the lipopolymer at the PEG-lipid junction contributes a surface charge density $\sigma_b = z_h e\beta$, where the valence $z_h = -1$ and the lipopolymer surface number density $\beta = c/A_l$ with $A_l \approx 0.6$–0.7 nm^2 the average lipid cross-sectional area.[14] Another charge with valence $z_t = -1$ resides at the free end of the PEG chain. We assume these charges uniformly sample the layer with thickness L, thereby endowing the polymer layer with a uniform charge density $\rho_p = z_t e\beta/L$. We let $L = 2R = 2lN^{1/2} \approx 7.52$ nm, where R is the PEG-chain unperturbed root-mean-squared end-to-end distance with $N \approx 28$ the number of statistical segments per chain and $l \approx 0.71$ nm the statistical segment length.[25]

Counterions in the diffuse double layer are assumed to be Boltzmann distributed in the y-direction perpendicular to the bilayer. It follows that the contribution of the N counterion species to the diffuse charge is

$$\rho_c(y) = \sum_{j=1}^{N} z_j e n_j^{\infty} \exp\left(\frac{-z_j e\psi(y)}{k_B T}\right) \quad (1)$$

where n_j^{∞} is the bulk concentration of the jth ion with valence z_j, e is the fundamental charge, and k_BT is the thermal energy.

The equilibrium electrostatic potential $\psi(y)$ satisfies the well-known Poisson–Boltzmann equation, which we linearize in the usual manner (Debye–Hückel approximation) for $|\psi| < k_BT/e$, giving

$$\frac{d^2\psi}{dy^2} - \kappa^2\psi = -\frac{\rho_p}{\varepsilon\varepsilon_o} \quad (2)$$

where $\rho_t(y) = \rho_p + \rho_c(y)$ is the total (volume) charge density, and

$$\kappa^{-1} = \sqrt{\frac{k_B T \varepsilon\varepsilon_o}{2e^2 I}}$$

is the Debye length with I the ionic strength.† Eqn (2) is accompanied by Gauss's law applied as a boundary condition $-\varepsilon\varepsilon_o \mathrm{d}\psi/\mathrm{d}y|_{y=0} = \sigma_b$, which, consistent with the foregoing Debye–Hückel approximation, is equivalent to setting $\varepsilon\varepsilon_o\kappa\psi(y=0) = \sigma_b$. Recall, in our experiments, $\sigma_b = z_h e\beta$ is attributed only to the lipopolymers, since the supporting DOPC lipids are zwitterions with zero net charge.

In the absence of a longitudinal pressure gradient, fluid momentum conservation (in the absence of fluid inertia) demands

$$0 = \eta\frac{d^2u}{dy^2} + \rho_t(y)E - \gamma_s n_s(u - V) \quad (3)$$

where η is the (water) shear viscosity, $n_s = N\beta/L$ is the average statistical segment number density in the (uniform) polymer layer, $\gamma_s = 6\pi\eta a_s$ is the statistical-segment friction coefficient with Stokes hydrodynamic radius a_s, $u(y)$ is the (longitudinal) fluid velocity, and V is the polymer drift velocity. We assume a no-slip boundary condition $u = 0$ at $y = 0$, which, in turn, is motivated by an assumption that there is zero net bilayer drift. Thus, while charged lipids migrate under the influence of the electric field, a counter-flow of uncharged lipids—and an accompanying longitudinal bilayer pressure gradient—is generated spontaneously to maintain a constant lipid density.

† $I = 1/2\sum z_j^2 c_j$, where c is the bulk concentration of the jth ion with valence z_j. The buffer in electrophoresis experiments contains 0.5 mM Na_2HPO_4 and 0.25 mM NaH_2PO_4, with pH = 7.4 at 295 K. From the acid dissociation constants (pK_as) of H_3PO_4, $H_2PO_4^-$ and HPO_4^{2-}, and the buffer pH (pH changes due to electrophoresis are neglected), the concentrations of H_3PO_4, PO_4^{3-} and H^+ are negligible compared to those of HPO_4^{2-} and $H_2PO_4^-$, so we have 1.25 mM Na^+, 0.5 mM HPO_4^{2-}, and 0.25 mM $H_2PO_4^-$.

The lipopolymer equation of motion is

$$0 = (z_t + z_h)eE - \gamma_t V - \beta^{-1}\int_0^\infty \gamma_s n_s (V - u)\mathrm{d}y \quad (4)$$

where γ_t is the lipid-tail drag coefficient. Note that the total frictional force on the lipopolymer comprises the friction on the lipid (hydrocarbon) tail within the bilayer and the hydrodynamic drag on its polymer chain; these are the second and third terms, respectively, on the right-hand side of eqn (4).

Eqn (2)–(4) are easily solved using liner superposition‡to furnish an explicit formula for the lipopolymer electrophoretic mobility

$$\mu_E = V/E \quad (5)$$

Details of the analytical solution, including explicit expressions for the fluid and polymer velocities, are provided in the Appendix, and a typical set of model parameters is listed in Table 1. Note that our calculations accommodate electrical and hydrodynamic boundary conditions at the top surface of the electrophoresis channel. However, these boundary conditions do not influence μ_E in this work, because the channel height $H \approx 500\ \mu$m is significantly greater than $L + \kappa^{-1} \approx 20$ nm. Thus, we simply demand a vanishing equilibrium electrostatic potential $\psi \to 0$ and vanishing hydrodynamic shear stress $\eta\partial u/\partial y \to 0$ as $y \to \infty$.

Because our model is quasi-steady, it is valid only when a uniform membrane is subjected to a steady, uniform electric field. With lateral confinement, membranes eventually become inhomogeneous, approaching an equilibrium state with Boltzmann distributed energy where the lipopolymer diffusion flux balances electro-migration. This parallels the pioneering studies of Boxer and coworkers involving charged bilayers without lipopolymers.[11,12] The time scale to reach equilibrium is the time L_c/V for lipopolymers to drift across their lateral confinement distance L_c at velocity $V = \mu_E E$. We typically synthesized lipid bilayers with $L_c > 15$ mm. However, to ensure the bilayers under observation are continuous, is is reasonable to state that $L_c \geq 500\ \mu$m, which is the maximum field of view. The accompanying equilibrium time for lipopolymers with drift velocity $V \sim 100$ nm s^{-1} is therefore $\geq 5 \times 10^3$ s, which is considerably longer than the several seconds required to measure the electric-field-induced drift. Accordingly, the membranes can be reasonably considered as uniform on the measurement time scale. We also neglect the dynamics of establishing a quasi-steady hydrodynamic profile within the electrophoresis channel. This is the $\sim H^2/\nu \sim 0.04$ s momentum diffusion time scale, where $\nu \sim 10^{-6}$ m^2 s^{-1} is the fluid (water) kinematic viscosity. Clearly, this is much shorter than the ~ 1 s imaging time, so the electro-osmotic flow can indeed be considered quasi-steady.

Note that the foregoing linear relationship between surface potential and surface charge density breaks down at high lipopolymer concentrations, because the accompanying charge densities produce surface potentials greater than k_BT/e. Under these conditions, we adopt the well-known Gouy-Chapman equation[26]

$$\psi(y = 0) = \frac{2k_BT}{ze}\mathrm{asinh}\left(\frac{\sigma_b ze}{2\kappa\varepsilon\varepsilon_o k_B T}\right) \quad (6)$$

to calculate a surface potential $\psi(y = 0)$ corresponding to the specified surface charge density $\sigma_b = z_h e\beta$. This implicitly furnishes an *effective* or corrected surface charge density $|\sigma_e| = \varepsilon\varepsilon_s\kappa|\psi(y = 0)| < |\sigma_b|$.

To test this approximation, we solved the full model—with the non-linear Poisson–Boltzmann equation—numerically§ on the intervals $[0, L]$ and $[L, 50L]$. Boundary conditions at $y = 0$ and L are the same as for the analytical solution, but we applied the analytical solution evaluated at $y = 50L$ to furnish a far-field boundary condition for the numerical calculations. Fig. 1 confirms that the analytical solution based on the linearized Poisson–Boltzmann equation is accurate with lipopolymer concentrations $c \leq 1$ mol%. However, it overestimates the electro-osmotic drag at higher concentrations due to overestimating the surface potential from the specified surface charge density. Nevertheless, by correcting the surface potential with eqn (6), the analytical solution achieves satisfactory agreement with the numerical calculations at all lipopolymer concentrations. Accordingly, we interpreted our experimental data using the analytical solution with $\psi(y = 0)$ specified according to eqn (6) with $\sigma_b = z_h e\beta$.

Table 1 Summary of lipopolymer electrophoresis model parameters

PEG-chain molecular weight	M	2 kg mol^{-1}
PEG-chain statistical segments per chain	N	28
PEG-chain statistical segment length	l	0.71 nm
Lipid head cross-sectional area	A_l	0.65 nm^2
PEG chain mean-squared end-to-end distance	R	$lN^{1/2} \approx 3.76$ nm
PEG layer thickness	L	$2R$
Lipopolymer mole fraction	c	
Lipopolymer number density or PEG-chain grafting density	β	c/A_l
Bilayer surface charge density	σ_b	$z_h e\beta$
Lipid-tail friction coefficient	γ_t	
Lipopolymer area fraction	ϕ	βL^2
Hydrodynamic segment size	a_s	
Solvent dielectric constant	ε	78.5
Solvent viscosity	η	8.89 mPa s
Absolute temperature	T	295 K
Electrophoresis channel (top) surface charge density	σ_t	0
Electrophoresis channel height	H	500 μm
Electrolyte ionic strength	I	1.75 mM
Electrolyte Debye length	κ^{-1}	7.27 nm

2 Experimental

We conducted experiments with glass cover-slip supported bilayers doped with various concentrations of 1,2-distearoyl-sn-glycero-3-phosphoethanolamine-N-[poly(ethylene glycol)2000-N′-carboxyfluorescein] (DSPE-PEG2k-CF, Avanti Polar Lipids) in 1,2-dioleoyl-sn-glycero-3-phosphocholine (DOPC, Avanti

‡ We solved a sub-problem where the lipopolymers are translated at a specified velocity V in the absence of an electric field ($E = 0$), and another sub-problem where the lipopolymers are fixed ($V = 0$) in the presence of an electric field. These solutions are superposed to satisfy the polymer equation of motion (5) and, thus, determine μ_E.

§ The governing partial differential equations were solved using the Matlab function 'bvp4c'.

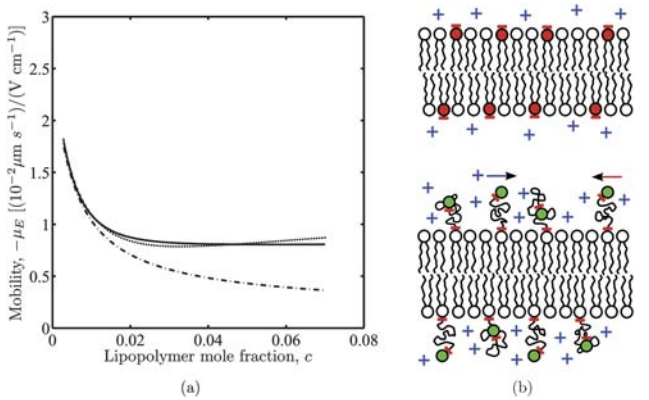

Fig. 1 (a) Theoretical calculations of lipopolymer (DSPE-PEG2k-CF) electrophoretic mobility $\mu_E = V/E$ as a function of its mole fraction c: $\gamma_t = D_t/(k_BT)$ with $D_t = 3.5\ \mu m^2\ s^{-1}$ and $a_s = 0.74\ \AA$. Other parameters are detailed in the text. The dashed line is the analytical solution with the Debye–Hückel approximation; the dotted line is the analytical solution corrected with the Gouy-Chapman equation; and the solid line is a numerical solution with the non-linear Poisson–Boltzmann equation. (b) Schematics of DOPE-NBD doped DOPC (top) and DSPE-PEG2k-CF doped DOPC (bottom) highlighting the negative (red) charges fixed to DOPE-NBD and DSPE-PEG2k-CF, and positive (blue) counterions. DOPC lipids are zwitterions with one positive and one negative charge (neither shown).

Polar Lipids). Bilayers were synthesized as described by Zhang & Hill.[27] Briefly, a mixture of lipids containing 2 mg DOPC and a specified concentration DSPE-PEG2k-CF in chloroform was dried under a stream of nitrogen gas, deep dried under vacuum for 2 h and reconstituted in buffer (10 mM phosphate, 100 mM NaCl, pH 7.4) to 2 mg mL^{-1}. The lipid mixture was extruded first through a 100 nm and then a 50 nm polycarbonate membrane (Avanti Polar Lipids) to form small unilamellar vesicles that we deposited on pre-treated cover-slips to form lipid bilayers by vesicle fusion. The cover-slips were first boiled in a detergent solution for 30 min, rinsed excessively in reverse osmosis (RO) water, dried under a stream of nitrogen gas, and finally Piranha etched for 20 min in a solution of 3 : 1 (v/v) concentrated sulfuric acid (H_2SO_4) and 30% hydrogen peroxide (H_2O_2) followed by rising in RO water and drying under a stream of nitrogen gas.

Fluid channels with dimensions 30 mm × 6 mm × 0.5 mm were constructed from polydimethylsiloxane (PDMS, Sylgard 184, Dow Corning) using a metal mold and mounted onto a precleaned cover-slip used as the bilayer support. Two platinum (Pt) electrodes were placed in PBS buffer reservoirs at the ends of the channel. A low ionic strength buffer containing 0.5 mM of Na_2HPO_4 and 0.25 mM of NaH_2PO_4 was used during electrophoresis to reduce Joule heating. The pH is ~ 7.4 and, recall, the ionic strength is ~ 1.75 mM. For an electric field strength less than 100 V cm^{-1}, the temperature increase was calculated to be less than 0.5 °C min^{-1}, and can therefore be neglected. The electric field strength was calculated from knowledge of the current (available from the power supply, PS325, Stanford Research Systems), the conductivity of the diluted buffer (measured using a Zetasizer Nano Series instrument, Malvern Instruments Ltd.), and the channel cross-sectional area (estimated from the the mold used to cast the PDMS channel). Bilayers were imaged using a Zeiss LSM 5 confocal microscope fitted with a 63 ×/1.4 oil-immersion objective and a 488 nm argon ion laser operating at 0.1–0.5% intensity. The lipopolymer drift velocity was obtained by imaging a photo-bleached stripe[28] with the sample carefully aligned to ensure horizontal electromigration across the field of view. The stripe was photo-bleached at 100% laser intensity in less than 100 ms, and its electromigration recorded and analyzed using the Zen software (Carl Zeiss) to obtain fluorescence intensity time series. The stripe center was accurately identified by fitting a Gaussian function to the vertically averaged fluorescence intensity line scans. Plotting the position *versus* time yielded a straight line whose slope is the DSPE-PEG2k-CF lipopolymer electromigration velocity V.

Control experiments were undertaken with 0.5 mol% 1,2-dioleoyl-sn-glycero-3-phosphoethanolamine-N-(7-nitro-2-1,3-benzoxadiazol-4-yl) (ammonium salt) (DOPE-NBD, Avanti Polar Lipids) in DOPC with various concentrations of 1,2-distearoyl-sn-glycero-3-phosphoethanolamine-N-[methoxy(polyethylene glycol)-2000] (ammonium salt) (DSPE-PEG2k, Avanti Polar Lipids).

3 Results and discussion

3.1 Measured lipopolymer electrophoretic mobility

A representative time series of bilayer images is shown in Fig. 2 (a). Lipopolymer self-diffusion broadens the vertical photo-bleached stripe.[28,29] While the self-diffusion coefficient can be ascertained from the broadening dynamics, this yields higher self-diffusion coefficients than obtained from fluorescence recovery after photobleaching (FRAP) experiments with a stationary, circular bleached spot. This is because the high illumination intensities required to accurately track the electric-field-induced drift yield (non-linear) photobleaching artifacts. Nevertheless, because photo-bleaching does not break the fore-aft symmetry, the observed drift velocity is independent of photo-bleaching. Representative photo-intensity profiles are shown in Fig. 2 (b). Least-squares Gaussian fits [*e.g.*, panel (c)] accurately identify the translating mid-point, whose time dependence yields the lipopolymer electrophoretic drift velocity V [panel (d)]. We selected the initial photo-bleaching width $w \approx 5\ \mu m$ and depth to optimize the signal-to-noise ratio. Note that the characteristic recovery time is the $\sim w^2/D_s \sim 30$ s diffusion time, which is considerably longer than the several seconds required to accurately track the drift. Plotting the drift velocity V as a function of the electric field strength E yields a straight line whose slope is the electrophoretic mobility $\mu_E = V/E$. In Fig. 3, for example, $\mu_E \approx -0.016\ (\mu m\ s^{-1})/(V\ cm^{-1})$ is obtained with $c \approx 0.5$ mol% DSPE-PEG2k-CF in DOPC.

Electrophoretic mobilities μ_E of lipopolymer DSPE-PEG2k-CF in DOPC are plotted as a function of its mole fraction c in Fig. 4 (a) (circles). Also shown are the mobilities of 0.5 mol% DOPE-NBD in DOPC with various DSPE-PEG2k mole fractions c (squares). The negative sign corresponds to the negative lipid valences: $z = -2$ for DSPE-PEG2k-CF and $z = -1$ for DSPE-PEG2k. Moreover, the monotonic decrease in the DSPE-PEG2k-CF mobility magnitude with increasing concentration indicates that the migration is hindered, either because of direct

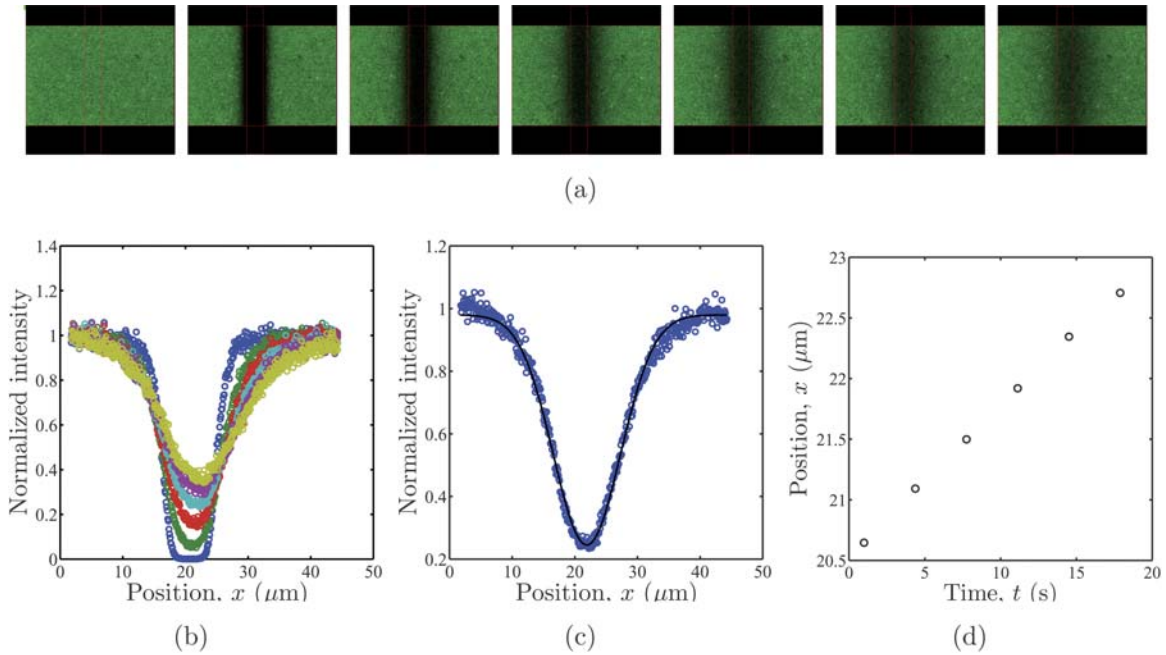

Fig. 2 Lipopolymer electrophoresis in supported lipid bilayers. (a) Representative fluorescence images of DSPE-PEG2k-CF in DOPC under the influence of a horizonal electric field at times $t \approx 0$, 1.0, 4.4, 7.5, 11.1, 14.5, 17.9 s (left-to-right). The scale is set by the initial width $w \approx 5$ μm of the (vertical) photo-bleached strip. (b) Vertically averaged photo-intensity profiles at times $t \approx 0$, 3.4, 6.5, 10.1, 13.5 and 16.9 s after photobleaching. Intensity is normalized with the intensity immediately before photobleaching [first image in panel (a)]. (c) A representative Gaussian fit to the vertically averaged photo-intensity profile at $t \approx 10.1$ s after photobleaching. (d) An electrophoretic drift velocity $V \approx 0.12$ μm s^{-1} is deduced from the linear dependence of position on time with $c \approx 0.5$ mol% and $E \approx -14$ V cm^{-1}).

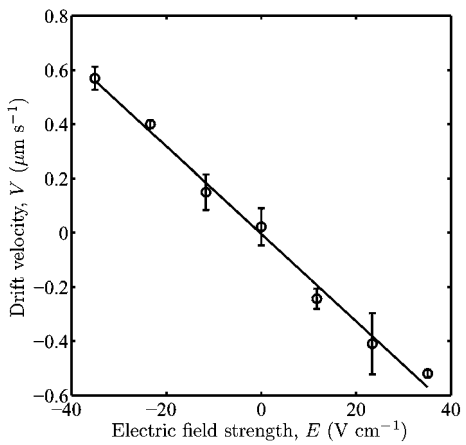

Fig. 3 Lipopolymer DSPE-PEG2k-CF electrophoretic drift velocity V as a function of the electric field strength E with lipopolymer concentration $c \approx 0.5$ mol% in DOPC. Error bars are the standard deviation from three measurements of V at each value of E. Here, the electrophoretic mobility $\mu_E \approx -0.016$ (μm s^{-1})/(V cm^{-1}).

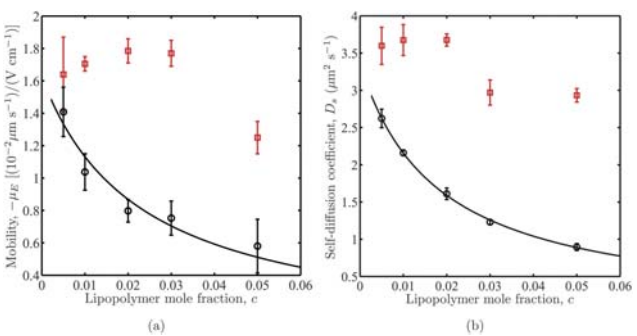

Fig. 4 (a) Electrophoretic mobilities μ_E of lipopolymer DSPE-PEG2k-CF in DOPC as a function of the lipopolymer mole fraction c (circles). Also shown are the electrophoretic mobilities of 0.5 mol% DOPE-NBD in DOPC with DSPE-PEG2k mole fractions c (squares). (b) Self-diffusion coefficients D_s of DSPE-PEG2k-CF in DOPC as a function of its mole fraction c (circles).[27] Also shown are self-diffusion coefficients of 0.5 mol% DOPE-NBD in DOPC with DSPE-PEG2k mole fractions c (squares). Error bars are the standard deviation of two or three data sets at each lipopolymer concentration, and the solid lines in panels (a) and (b) are, respectively, eqn (8) and (9) fitted to the DSPE-PEG2k-CF data.

hydrodynamic and thermodynamic interactions or because of coupling to the oppositely directed electro-osmotic flow. Fitting an empirical formula

$$\mu_E = \mu_E{}^0/(1 + \alpha c) \quad (7)$$

to the DSPE-PEG2k-CF mobility data furnishes $\mu_E{}^0 = -1.6 \times 10^{-2}$ μm s^{-1}/(V cm^{-1}) and $\alpha = 44$ (solid line) with c expressed as a mole fraction.

The mobilities of the 0.5 mol% DOPE-NBD control have a much weaker dependence on lipopolymer concentration at DSPE-PEG2k concentrations $c \leq 4$ mol%. The slight increase with DSPE-PEG2k concentration at low concentrations suggests that the DOPE-NBD mobility might be enhanced by coupling to DSPE-PEG2k disturbances within the bilayer. Alternatively, the increase might be due to DSPE-PEG2k in the bottom leaflet

increasing the bilayer-support separation, thereby reducing hydrodynamic coupling to the solid support. At higher DSPE-PEG2k concentrations, the mobility decreases, as might be expected from coupling to electro-osmotic flow driven by the increasing DSPE-PEG2k counter charge density.

Interestingly, the electrophoretic mobilities of 0.5 mol% DOPE-NBD and DSPE-PEG2k-CF are comparable in the limit of vanishing lipopolymer concentration, even though DSPE-PEG2k-CF bears twice the charge as DOPE-NBD. Thus, the terminal charge on DSPE-PEG2k-CF seems to have a negligible influence on the lipopolymer mobility. Surprisingly, the DOPE-NBD and DSPE-PEG2k-CF mobilities reflect a dominant balance of the electrical force on the lipid head ($z_h = -1$ for both lipids) and the drag force on the (hydrocarbon) lipid tail. Evidently, the electrical force on the polymer chain is balanced by hydrodynamic coupling to electro-osmotic flow.

Self-diffusion coefficients D_s of lipopolymer DSPE-PEG2k-CF in DOPC are plotted as a function of its mole fraction c in Fig. 4 (b) (circles). These data are taken from Zhang & Hill,[27] who attributed the hindered self-diffusion coefficient at small, but finite, concentrations to soft repulsive thermodynamic interactions between the PEG chains. Also shown are the self-diffusion coefficients of 0.5 mol% DOPE-NBD in DOPC with various DSPE-PEG2k mole fractions c (squares). As shown by Zhang & Hill,[27] the DSEP-PEG2k-CF self-diffusion coefficient is well represented by the empirical formula

$$D_s = D_0/(1 + \alpha c) \tag{8}$$

where $D_0 \approx 3.36\ \mu m^2\ s^{-1}$ and $\alpha \approx 56$ with c expressed as a mole fraction. By the well-known Stokes–Einstein relationship, this corresponds to a drag coefficient $\gamma = k_BT/D_s(c)$ that increases linearly with lipopolymer concentration (see Fig. 7).

Accordingly, if the electrical force is assumed constant and balanced by only frictional drag, then the electrophoretic mobility would have the same concentration dependence as the self-diffusion coefficient. This is qualitatively confirmed by the DSPE-PEG2k-CF electrophoretic mobilities and self-diffusion coefficients shown in Fig. 4 (a) and (b), respectively. However, we will see that the quantitative differences can be attributed to electro-osmotic flow. Similarly to the 0.5 mol% DOPE-NBD electrophoretic mobilities in panel (a), the 0.5 mol% DOPE-NBD self-diffusion coefficient has a weak dependence on DSPE-PEG2k concentration. While the DOPE-NBD self-diffusion coefficient increases slightly with DSPE-PEG2k concentration at low lipopolymer concentrations, the self-diffusion coefficient is slightly hindered at higher DSPE-PEG2k concentrations. At least qualitatively, these variations can be attributed to the same mechanisms that influence the electrophoretic mobility.

To expedite a quantitative relationship between μ_E as D_s, let us consider the electrical force zeE balancing the drag force Vk_BT/D_s furnished by the the Stokes–Einstein relationship. This yields an electrophoretic mobility

$$\mu_D = \frac{zeD_s}{k_BT} \tag{9}$$

that is not necessarily equal to the actual electrophoretic mobility $\mu_E = V/E$. Indeed, Stelzle *et al.*[13] reported $\mu_E/\mu_D \approx 0.6$ for DOPE-NBD in the absence of lipopolymer, attributing the deviation from unity to electro-osmotic flow. Similarly, McLaughlin & Poo[4] found that concanavalin-A receptors on embryonic muscle cells that normally accumulate at the cathode side of the cell can be induced to accumulate either at the anode side by reducing the negative charge (decreasing the electrophoretic force) or at the cathode side by adding negative charge to the cell surface (increasing the electroosmotic force). Since the bulk lipids (DOPC) in our SLBs have zero net charge, the negatively charged lipopolymers (DSPE-PEG2k-CF and DSPE-PEG2k) endow the layers with a surface charge density $\sigma < 0$ whose magnitude is proportional to the respective lipopolymer concentration. Therefore, the accompanying ζ-potentials are negative, and the accompanying electroosmotic flow slows the electrophoretic drift of DSPE-PEG2k-CF, DSPE-PEG2k, and 0.5 mol% DOPE-NBD.

The DSPE-PEG2k-CF electrophoretic mobility μ_E (circles) is plotted with μ_D (squares) in Fig. 5 (a). Also shown are μ_E (up-triangles) and μ_D (right-triangles) for 0.5 mol% DOPE-NBD in DOPC with various DSPE-PEG2k mole fractions c. While the DSPE-PEG2k-CF electrophoretic mobilities μ_E are ostensibly lower than their respective μ_D, the 0.5 mol% DOPE-NBD mobilities μ_E are somewhat higher their respective μ_D. The ratios μ_E/μ_D are plotted in Fig. 5 (b), where the significant deviations from unity indicate that electro-osmosis, which is absent in the specification of μ_D, plays an important role.

The ratio μ_E/μ_D for DSPE-PEG2k-CF is approximately independent of concentration, suggesting that the dominant influence of electro-osmotic flow is independent of lipid interactions. Thus, as expected, the DSPE-PEG2k-CF mobility μ_E is hindered by electro-osmotic flow. The nominal value $\mu_E/\mu_D \sim 0.7$ confirms inferences above that the electrical force on the free end of the PEG chain is balanced by hydrodynamic coupling of the PEG chains to electro-osmotic flow driven by the mobile counter charges. If this coupling were perfect, *i.e.*, the electrical force were exactly balanced by the hydrodynamic retardation force, then the effective DSPE-PEG2k-CF valence would be reduced to $z = -1$; rather, the effective valence $z \approx -1.4$ suggests an $\sim 60\%$ reduction in the apparent electrical force.

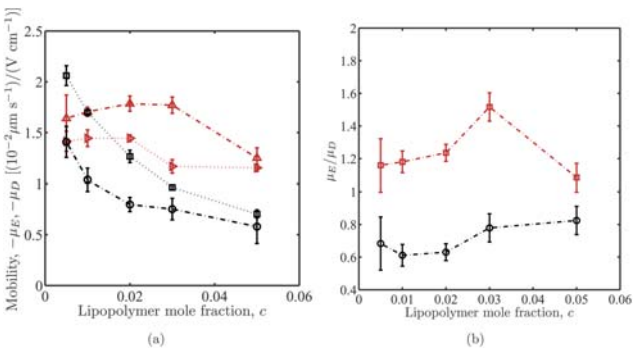

Fig. 5 Interpreting electrophoretic mobilities with knowledge of self-diffusion coefficient. (a) Actual electrophoretic mobilities μ_E (circles) and electrophoretic mobilities μ_D (squares) of DSPE-PEG2k-CF in DOPC with DSPE-PEG2k-CF mole fractions c. Also shown are μ_E (up-triangles) and μ_D (right-triangles) of 0.5 mol% DOPE-NBD in DOPC with DSPE-PEG2k mole fractions c. (b) μ_E/μ_D for DSPE-PEG2k-CF (circles) and 0.5 mol% DOPE-NBD (squares) in DOPC with lipopolymer mole fractions c. Lines are to guide the eye.

In striking contrast, $\mu_E/\mu_D \sim 1.2 > 1$ for 0.5 mol% DOPE-NBD, so electrical influences evidently enhance the electrophoretic mobility. This might be due to the accompanying DSPE-PEG2k electro-migration. Since the DOPE-NBD head presents a much smaller hydrodynamic size than the PEG2k chains on DSPE-PEG2k, it is likely to be more susceptible to hydrodynamic disturbances within the bilayer rather than above it. Thus, the collective electro-migration of DSPE-PEG2k tails within the leaflet might enhance DOPE-NBD electro-migration. Note that this can only occur if there exists a positive correlation between DOPE-NBD and DSPE-PEG2k concentration fluctuations, thereby demanding an attractive contribution to the interaction between DOPE-NBD and DSPE-PEG2k. The electrostatic interaction is obviously repulsive over separation distances on the order of the Bjerrum length (~ 0.7 nm), so an attractive interaction would have to arise from the PEG2k interaction with NBD. Alternatively, such correlations might be facilitated by local fluctuations of bilayer curvature.

3.2 Theoretical interpretation

The theoretical model, evaluated with a constant lipid-tail drag coefficient, was demonstrated in Fig. 1 to yield a lipopolymer electrophoretic mobility that decreases monotonically with increasing lipopolymer concentration. This is clearly in good qualitative agreement with the foregoing experiments with lipopolymer DSPE-PEG2k-CF in DOPC. Our model assigns a lipid-tail drag coefficient and separately calculates the drag force on the PEG chains *via* a Brinkman (continuum) model of the polymer layer with uniform charge density and hydrodynamic permeability. Even with these approximations, there are several model parameters that must be specified to expedite a quantitative comparison of the theory and experiment. These parameters include the lipid-tail drag coefficient γ_t, polymer layer thickness L, and hydrodynamic permeability ℓ_B^2, all of which may vary with lipopolymer concentration.

To assess the layer thickness and density, we performed self-consistent mean-field calculations furnishing the segment-density distributions shown in Fig. 6. Even at the highest lipopolymer concentration $c \approx 5$ mol%, the layers have Gaussian profiles rather than the parabolic profiles that are characteristic of brushes when the area fraction $\phi \sim \beta(2R)^2 \geq 1$. Thus, the characteristic layer thickness is independent of the lipopolymer concentration, and is well approximated by twice the unperturbed root-mean-squared end-to-end distance, *i.e.*, $L = 2R = 2lN^{1/2} \approx 7.52$ nm, as adopted in section 1. Accordingly, the uniform layers in our electrokinetic model have a segment density $n_s = \beta N/L = cN/(LA_l)$. For PEG2k, the number of statistical segments $N = 28$, and the segment length $l = 0.71$ nm.[25]

Having specified the polymer layer thickness, we compute the hydrodynamic permeability by assigning a Stokes hydrodynamic radius a_s to each statistical segment. Thus, the hydrodynamic drag force per unit volume, $6\pi\eta a_s n_s[u(y) - V] \equiv \eta\ell_B^{-2}[u(y) - V]$, yields a hydrodynamic permeability (square of the Brinkman screening length)

$$\ell_B^2 = \frac{1}{\pi a_s n_s} = \frac{L}{6\pi a_s \beta N} = \frac{l}{3\pi a_s \beta N^{1/2}} \tag{10}$$

Accordingly, by specifying l, N, and $\beta = c/A_l$, we consider the Stokes radius a_s as a fitting parameter.

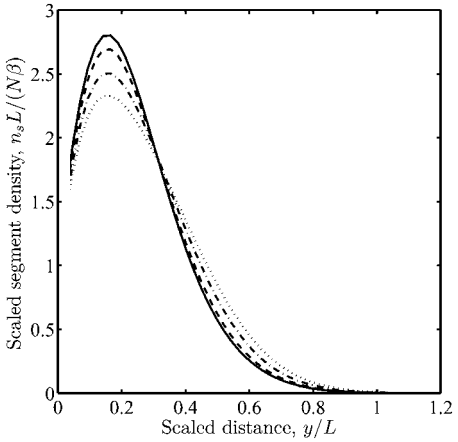

Fig. 6 Scaled polymer segment density distributions $n_sL/(N\beta)$ for various scaled polymer grafting densities (area fractions) $\phi = \beta L^2$, where $L = 2R = 2lN^{1/2}$, according to self-consistent mean field theory with Flory parameter $\chi = 0.47$. Note that the dimensional segment density n_s is scaled with $N\beta/L$, the value for a uniform profile with thickness $L = 2R = 2lN^{1/2}$, and distance from the (flat) grafting surface y is scaled with L. Lines identify scaled grafting densities (area fraction) $\phi = \beta L^2 \approx 0.43$ (solid), 1.74 (dashed), 4.24 (dash-dotted), and 6.95 (dotted).

Now consider the lipid tail drag coefficient γ_t. Again, we turn to the Stokes–Einstein relationship. However, because our electrokinetic model accounts for frictional forces on the polymer, the lipid-tail drag coefficient must be ascertained from the DOPE-NBD self-diffusion coefficient, since the drag force on these lipids is predominantly from the hydrocarbon tail. Nevertheless, even the DOPE-NBD drag coefficient may be influenced by bilayer-polymer hydrodynamic coupling. We therefore assess the lipid-tail drag coefficient from the Stokes–Einstein interpretation of the 0.5 mol% DOPE-NBD self-diffusion coefficient in the presence of DSPE-PEG2k with mole fraction c. This data, which is presented in Fig. 4, confirms that the drag coefficient $\gamma_t = k_BT/D_s$ is a much weaker function of the lipopolymer concentration than the drag coefficient of the lipopolymer itself. Fig. 7 shows the drag coefficients of DSPE-PEG2k-CF and 0.5 mol% DOPE-NBD as a function of the lipopolymer concentration, each normalized by its respective value γ_0 at infinite lipopolymer dilution. From the empirical form of the self-diffusion coefficient proposed by Zhang & Hill,[27] the drag coefficient increases linearly with lipopolymer concentration, with a slope that reflects thermodynamic and hydrodynamic interactions.

For DSPE-PEG2k-CF, the self-diffusion coefficient correlated by Zhang & Hill[27] gives $\gamma/\gamma_0 \approx 1 + 56c$, where c the DSPE-PEG2k-CF mole fraction. Note that an excellent fit of our electrokinetic model for the DSPE-PEG2k-CF electrophoretic mobility is furnished by a concentration dependent lipid-tail drag coefficient

$$\gamma_t/\gamma_0 \approx 1 + 5c \tag{11}$$

where $\gamma_0 = k_BT/D_0 \approx 1.16 \times 10^{-9}$ kg s^{-1} and c is expressed as a mole fraction. Here, $D_0 = 3.5$ μm^2 s^{-1} is a reasonable estimate of DOPE-NBD and DSPE-PEG2k-CF self-diffusion coefficients at infinite lipopolymer dilution. Recall, lipopolymer

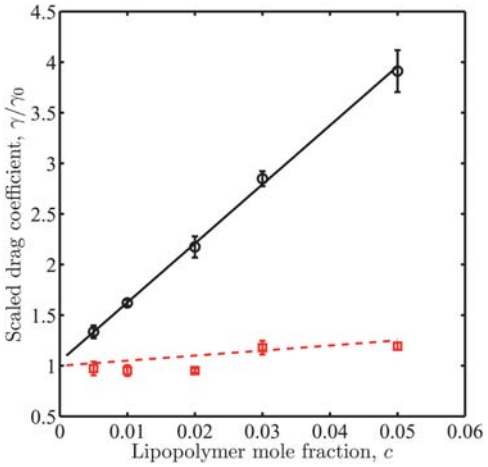

Fig. 7 Scaled drag coefficients $\gamma/\gamma_0 = D_0/D_s$ of DSPE-PEG2k-CF in DOPC with DSPE-PEG2k-CF mole fractions c (circles), and 0.5 mol% DOPE-NBD in DOPC with DSPE-PEG2k mole fractions c (squares). The solid line is $\gamma/\gamma_0 = 1 + 56c$ obtained directly from DSPE-PEG2k-CF self-diffusion coefficients,[27] and the dashed line is $\gamma/\gamma_0 = 1 + 5c$ obtained indirectly from the DSPE-PEG2k-CF electrophoretic mobilities interpreted with the continuum electrophoresis model.

self-diffusion coefficients at infinite dilution are practically independent of the grafted PEG2k chains.[27] As shown in Fig. 7, eqn (11) (dashed line) is compatible with the lipopolymer concentration dependence of the 0.5 mol% DOPE-NBD friction coefficient (squares) inferred from the self-diffusion coefficient in SLBs with varying concentrations of DSPE-PEG2k.

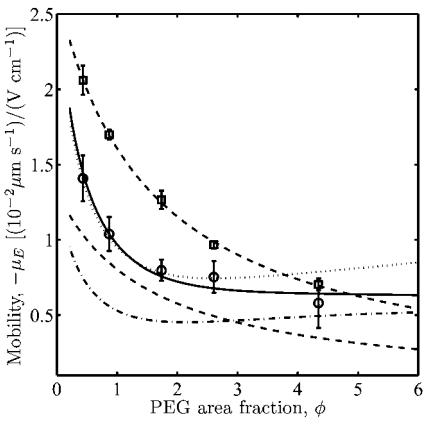

Fig. 8 The electrophoretic mobility μ_E of lipopolymer DSPE-PEG2k-CF as a function of the scaled lipopolymer concentration $\phi = cL^2/A_l = \beta L^2$. Circles are the experimental data; the dotted line is the theory with PEG-chain statistical-segment Stokes radius $a_s = 0.86$ Å and a constant lipid-tail drag coefficient $\gamma_t = k_BT/D_0$ with $D_0 = 3.5\ \mu m^2\ s^{-1}$; the solid line is the theory with $a_s = 0.74$ Å and a lipid-tail drag coefficient $\gamma_t = (1 + 5c)k_BT/D_0$ with $D_0 = 3.5\ \mu m^2\ s^{-1}$; and the upper dashed line is the electrophoretic mobility μ_D predicted from the concentration dependence of the lipopolymer self-diffusion coefficient.[27] The dash-dotted line is a theoretical prediction of the electrophoretic mobility of DSPE-PEG2k in DOPC, and the lower dashed line is the electrophoretic mobility μ_D predicted from the concentration dependence of the DSPE-PEG2k-CF self-diffusion coefficient.[27]

Fig. 8 compares the DSPE-PEG2k-CF electrophoretic mobility predicted by our electrophoresis model (solid and dotted lines) with the experimental data (circles). The parameters adopted for these calculations are listed in Table 1. The theoretical calculations shown as the dotted line have a constant lipid-tail drag coefficient $\gamma_t = k_BT/D_0$ with $D_0 = 3.5\ \mu m^2\ s^{-1}$, and $a_s = 0.86$ Å as a single fitting parameter. There is a good correspondence at low lipopolymer concentrations, but an erroneous increase at higher concentrations suggests that the lipid-tail drag coefficient actually increases with lipopolymer concentration, as corroborated by Fig. 7. Accordingly, calculations with a lipid-tail drag coefficient $\gamma_t = (1 + 5c)k_BT/D_0$ with $D_0 = 3.5\ \mu m^2\ s^{-1}$, and $a_s = 0.74$ Å the single fitting parameter, produce an excellent fit over the entire range of lipopolymer concentrations.

For convenient reference, Fig. 8 also shows the electrophoretic mobility μ_D predicted using the self-diffusion coefficient reported by Zhang & Hill[27] (dashed line). As discussed above, this does not account for electro-osmotic flow, and, thus, over-predicts the mobility at low lipopolymer concentrations, and under-predicts the mobility at high concentrations. In fact, the theoretically predicted mobility μ_E at high concentrations appears to approach a finite value at high lipopolymer concentrations, whereas the electrophoretic mobility μ_D vanishes. It is not clear whether the correlation of Zhang and Hill can be extrapolated beyond $c \approx 5$ mol%, since the PEG-chains are expected to adopt increasingly extended, brush-like configurations at high enough lipopolymer concentrations, which may furnish a non-linear dependence of the drag coefficient on lipopolymer concentration.

Nevertheless, the finite lipopolymer electrophoretic mobility at high concentrations can be attributed to the linear increase of the electrical and hydrodynamic forces on the polymer layer with concentration. Recall, with fixed layer thickness, the electrical charge density and segment concentration are each proportional to the lipopolymer concentration (in the mean-field approximation). On the other hand, the electrophoretic mobility μ_D comes from balancing the constant electrical force per lipopolymer with a lipopolymer drag coefficient that increases approximately linearly with lipopolymer concentration.[27] Thus, our theoretical model and experiments identify a fundamental difference between the drag forces operating on a lipid as predicted by the Stokes–Einstein interpretation of the self-diffusion coefficient and the drag forces operating during collective electro-migration under the influence of electrical forces and electro-osmotic flow.

Finally, we have plotted in Fig. 8 theoretical predictions of the DSPE-PEG2k electrophoretic mobility in DOPC (dash-dotted line). These calculations were undertaken with the same parameters as for DSPE-PEG2k-CF, but with zero charge at the free PEG end. Here, the electro-osmotic flow is driven entirely by the counter charge of the lipid-PEG junction. As expected, the mobility μ_E is much closer to the electrophoretic mobility μ_D predicted from the lipid valence $z = -1$ and friction coefficient from the self-diffusion coefficient.[27] Interestingly, such a close correspondence prevails even though the calculation of μ_E does not draw upon explicit empirical knowledge of how the self-diffusion coefficient is modulated by the grafted PEG chain. Surprisingly, lipopolymer self-diffusion coefficients, which are successfully calculated on the basis of thermodynamics in the dilute limit, are reasonably well approximated by the drag

coefficient for collective translation, as furnished by the Brinkman model in our study.

4 Conclusions

We developed a continuum electrophoresis model for lipopolymers in supported lipid bilayer membranes, and used this model to interpret experimental measurements of the electrophoretic mobility of lipopolymer DSPE-PEG2k-CF in DOPC. Similarly to our earlier report of the concentration dependence of the self-diffusion coefficient, the experiments revealed an electrophoretic mobility that decreases monotonically with increasing concentration. To a first (qualitative) approximation, the electrophoretic mobility can be estimated by balancing the electrical force zeE with the hydrodynamic drag force Vk_BT/D_s furnished by the Stokes–Einstein interpretation of the self-diffusion coefficient $D_s(c)$.

However, quantitative comparison of theory and experiment at finite lipopolymer concentrations demands that electroosmotic flow and hydrodynamic coupling are accounted for. We obtained excellent agreement between the continuum electrophoresis model and experiments by calculating the hydrodynamic drag on the polymer chains according to a Brinkman model. This accounts for polymer layer thickness and polymer-segment density, and allows the lipid-tail drag coefficient to increase linearly with DSPE-PEG2k-CF concentration, *i.e.*, $\gamma_t = (1 + 5c)k_BT/D_s$, where $D_0 = 3.5\ \mu m^2\ s^{-1}$ and c is the lipopolymer mole fraction.

Finally, we complemented lipopolymer electrophoresis data with control experiments measuring the self-diffusion coefficients and electrophoretic mobilities of DOPE-NBD (a non-PEGylated, charged, fluorescent lipid) at low concentration (0.5 mol%) in DOPC bilayers with varying lipopolymer DSPE-PEG2k concentrations. These data support several interpretations of the lipopolymer experiments and modeling, and reveal many weaker and much more subtle interactions that prevail in these intriguing quasi-two-dimensional fluids.

A Analytical solution of the electrophoresis model

The electrophoresis channel comprises a domain inside the polymer layer, extending from the bilayer surface at $y = 0$ to the polymer-layer edge at $y = L$; and a domain outside the polymer layer, extending from $y = L$ to the channel top surface at $y = H$. In the fluid domain, the polymer segment density $n_s = 0$. We neglect the finite bilayer thickness, because it is small compared to the polymer layer thickness $L \sim 10$ nm and channel height $H \sim 500\ \mu m$.

As detailed in the main text, three coupled equations must be solved:

$$\frac{d^2\psi}{dy^2} - \kappa^2\psi = -\frac{\rho_p}{\varepsilon\varepsilon_o} \tag{12}$$

$$0 = \eta\frac{d^2u}{dy^2} + \rho_t(y)E - \gamma_s n_s(u - V) \tag{13}$$

$$0 = (z_t + z_h)eE - \gamma_t V - \beta^{-1}\int_0^\infty \gamma_s n_s(V - u)dy \tag{14}$$

The general solution of eqn (12) in the bilayer domain (with $\rho_p = z_h\beta e/L$) is

$$\psi = C_1e^{ky} + C_2e^{-ky} + \frac{z_he\beta}{\varepsilon\varepsilon_oL\kappa^2} \tag{15}$$

and in the fluid domain (with $\rho_p = 0$)

$$\psi = C_3e^{ky} + C_4e^{-ky} \tag{16}$$

The constants C_1–C_4 are fixed by the following boundary conditions. At $y = 0$,

$$\frac{d\psi}{dy}\Big|_{y=0} = -\frac{\sigma_b}{\varepsilon\varepsilon_o} \tag{17}$$

where σ_b is the bilayer surface charge density. At $y = H$,

$$\frac{d\psi}{dy}\Big|_{y=H} = -\frac{\sigma_t}{\varepsilon\varepsilon_o} \tag{18}$$

where σ_t is the electrophoresis channel surface charge density. Finally, at $y = L$,

$$\psi(L + \delta) = \psi(L - \delta) \tag{19}$$

and

$$\frac{d\psi}{dy}\Big|_{y=L+\delta} = \frac{d\psi}{dy}\Big|_{y=L-\delta} \tag{20}$$

as $\delta \to 0$.

These give

$$C_3 = \frac{1}{\varepsilon\varepsilon_o\kappa}\left[\frac{1}{e^{2\kappa H} - 1}\left(\frac{z_he\beta e^{\kappa L}}{2\kappa L} - \frac{z_he\beta e^{-\kappa L}}{2\kappa L} + \sigma_b\right) - \frac{\sigma_t}{e^{\kappa H} - e^{-\kappa H}}\right] \tag{21}$$

$$C_1 = C_3 - \frac{z_he\beta e^{-\kappa L}}{\varepsilon\varepsilon_o 2\kappa^2 L} \tag{22}$$

$$C_2 = C_1 + \frac{\sigma_b}{\varepsilon\varepsilon_o\kappa} \tag{23}$$

$$C_4 = C_2 + \frac{z_he\beta e^{\kappa L}}{\varepsilon\varepsilon_o 2\kappa^2 L} \tag{24}$$

Next, the solutions of eqn (14) and (15) are obtained from the linear superposition of the two simpler sub-problems detailed below.

In the E-problem, an electric field with strength $E \neq 0$ is applied with fixed lipopolymers, *i.e.*, $V = 0$. Accordingly,

$$0 = \eta\frac{d^2u^E}{dy^2} + \rho_p(y)E - \gamma_s n_s u^E \tag{25}$$

giving a force on each lipopolymer (linear in E)

$$f^E = (z_t + z_h)eE + \beta^{-1}\int_0^\infty \gamma_s n_s u^E dy \tag{26}$$

In the V-problem, lipopolymers are translated with a velocity $V \neq 0$ in the absence of an electric field, *i.e.*, $E = 0$. Accordingly,

$$0 = \eta \frac{d^2 u^V}{dy^2} - \gamma_s n_s (u^V - V) \tag{27}$$

giving a force on each lipopolymer (linear in V)

$$f^V = -\gamma_t V - \beta^{-1} \int_0^\infty \gamma_s n_s (V - u^V) dy \tag{28}$$

Finally, superposing these solutions to satisfy

$$f^V + f^E = 0 \tag{29}$$

gives the lipopolymer electrophoretic mobility

$$\mu_E = V/E = \frac{(z_t + z_h)e + \beta^{-1} \int_0^\infty \gamma_s n_s (u^E/E) dy}{\gamma_t + \beta^{-1} \int_0^\infty \gamma_s n_s (1 - u^V/V) dy} \tag{30}$$

The solution of eqn (25) in the polymer layer is

$$\begin{aligned} \frac{u^E}{E} =& C_5 e^{\lambda y} + C_6 e^{-\lambda y} + \frac{\kappa^2}{\kappa^2 - \lambda^2} \frac{\varepsilon\varepsilon_o}{\eta} C_1 e^{\kappa y} \\ &+ \frac{\kappa^2}{\kappa^2 - \lambda^2} \frac{\varepsilon\varepsilon_o}{\eta} C_2 e^{-\kappa y} + \frac{e\beta}{\lambda^2 \eta L} \end{aligned} \tag{31}$$

where the reciprocal Brinkman permeability

$$\lambda^2 = \gamma_s n_s / \eta \tag{32}$$

Outside the polymer layer,

$$u^E = C_7 y + C_8 + \frac{\varepsilon\varepsilon_o}{\eta} C_3 e^{\kappa y} + \frac{\varepsilon\varepsilon_o}{\eta} C_4 e^{-\kappa y} \tag{33}$$

The constants C_5–C_8 are specified by continuity of u^E and its gradient (shear stress) at $y = L$, and $u^E = 0$ (no slip) at $y = 0$ and H. The results are

$$C_6 = \frac{e^{\lambda L}(\lambda H - \lambda l + 1) A_1 + e^{\kappa L}(\kappa L - \kappa H - 1) A_2 + e^{-\kappa L}(\kappa H - \kappa L - 1) A_3 + A_4 - e/(N\gamma_s)}{e^{\lambda L}(\lambda L - \lambda H - 1) + e^{-\lambda L}(\lambda L - \lambda H + 1)} \tag{34}$$

$$C_5 = -(C_6 + A_1) \tag{35}$$

$$C_7 = -\lambda C_6 (e^{\lambda L} + e^{-\lambda L}) - \lambda e^{\lambda L} A_1 + \kappa e^{\kappa L} A_2 + \kappa e^{-\kappa L} A_3 \tag{36}$$

$$C_8 = -C_7 H + A_4 \tag{37}$$

where

$$A_1 = \frac{\varepsilon\varepsilon_o \kappa^2 C_1}{(\kappa^2 - \lambda^2)\eta} + \frac{\varepsilon\varepsilon_o \kappa^2 C_2}{(\kappa^2 - \lambda^2)\eta} + \frac{e}{N\gamma_s} \tag{38}$$

$$A_2 = \frac{\varepsilon\varepsilon_o \kappa^2 C_1}{(\kappa^2 - \lambda^2)\eta} - \frac{\varepsilon\varepsilon_o C_3}{\eta} \tag{39}$$

$$A_3 = \frac{\varepsilon\varepsilon_o \kappa^2 C_2}{(\kappa^2 - \lambda^2)\eta} - \frac{\varepsilon\varepsilon_o C_4}{\eta} \tag{40}$$

$$A_4 = -\frac{\varepsilon\varepsilon_o C_3 e^{\kappa H}}{\eta} - \frac{\varepsilon\varepsilon_o C_4 e^{-\kappa H}}{\eta} \tag{41}$$

The solution of eqn (27) in the polymer layer is

$$\frac{u^V}{V} = C_9 e^{\lambda y} + C_{10} e^{-\lambda y} + 1 \tag{42}$$

and outside the polymer layer

$$\frac{u^V}{V} = C_{11} y + C_{12} \tag{43}$$

The constants C_9–C_{12} are specified from the continuity of u^V and its gradient (shear stress) at $y = L$, and $u^V = 0$ (no slip) at $y = 0$ and H. The results are

$$C_{10} = \frac{1 - e^{\lambda L}(1 + \lambda H - \lambda L)}{e^{\lambda L}(1 - \lambda L + \lambda H) - e^{-\lambda L}(1 + \lambda L - \lambda H)} \tag{44}$$

$$C_9 = -C_{10} - 1 \tag{45}$$

$$C_{11} = -\lambda C_{10}(e^{\lambda L} + e^{-\lambda L}) - \lambda e^{\lambda L} \tag{46}$$

$$C_{12} = -C_{11} H \tag{47}$$

The electrophoretic mobility becomes

$$\mu_E = \frac{V}{E} = \frac{(z_t + z_h)e + \beta^{-1} \gamma_s n_s D_E}{\gamma_t + \beta^{-1} \gamma_s n_s D_V} \tag{48}$$

where

$$\begin{aligned} D_E =& \frac{C_5}{\lambda}(e^{\lambda L} - 1) + \frac{C_6}{\lambda}(1 - e^{-\lambda L}) + \frac{\varepsilon\varepsilon_o \kappa C_1}{(\kappa^2 - \lambda^2)\eta}(e^{\kappa L} - 1) \\ &+ \frac{\varepsilon\varepsilon_o \kappa C_2}{(\kappa^2 - \lambda^2)\eta}(1 - e^{-\kappa L}) + \frac{eL}{N\gamma_s} \end{aligned} \tag{49}$$

and

$$D_V = \frac{C_9}{\lambda}(1 - e^{\lambda L}) + \frac{C_{10}}{\lambda}(e^{-\lambda L} - 1) \tag{50}$$

Acknowledgements

R.J.H. gratefully acknowledges support from the Natural Sciences and Engineering Research Council of Canada and the Canada Research Chairs program; H.-Y.Z. thanks McGill University and the Faculty of Engineering, McGill University, for generous financial support through a Richard H. Tomlinson

Fellowship and a McGill Engineering Doctoral Award (Hatch Graduate Fellowships in Engineering), respectively.

References

1 L. F. Jaffe, *Nature*, 1977, **265**, 600–602.
2 M.-M. Poo and K. R. Robinson, *Nature*, 1977, **265**, 602–605.
3 M.-M. Poo, J. W. Lam, N. Orida and A. W. Chao, *Biophys. J.*, 1979, **26**, 1–21.
4 S. McLaughlin and M.-M. Poo, *Biophys. J.*, 1981, **34**, 85–93.
5 T. A. Ryan, J. Myers, D. Holowka, B. Baird and W. W. Webb, *Science*, 1988, **239**, 61–64.
6 M.-M. Poo, *Annu. Rev. Biophys. Bioeng.*, 1981, **10**, 245–276.
7 E. Sackmann, *Science*, 1996, **271**, 43–48.
8 J. T. Groves, S. G. Boxer and H. M. McConnell, *Proc. Natl. Acad. Sci. U. S. A.*, 1997, **94**, 13390–13395.
9 J. T. Groves, S. G. Boxer and H. M. McConnell, *Proc. Natl. Acad. Sci. U. S. A.*, 1998, **95**, 935–938.
10 K. Y. C. Lee, J. F. Klingler and H. M. McConnell, *Science*, 1994, **263**, 655–658.
11 J. T. Groves and S. G. Boxer, *Biophys. J.*, 1995, **69**, 1972–1975.
12 J. T. Groves, C. Wülfing and S. G. Boxer, *Biophys. J.*, 1996, **71**, 2716–2723.
13 M. Stelzle, R. Miehlich and E. Sackmann, *Biophys. J.*, 1992, **63**, 1346–1354.
14 D. Marsh, R. Bartucci and L. Sportelli, *Biochim. Biophys. Acta, Biomembr.*, 2003, **1615**, 33–59.
15 M. Tanakan and E. Sackmann, *Nature*, 2005, **437**, 656–663.
16 F. Albertorio, A. J. Diaz, T. Yang, V. A. Chapa, S. Kataoka, E. T. Castellana and P. S. Cremer, *Langmuir*, 2005, **21**, 7476–7482.
17 F. Albertorio, S. Daniel and P. S. Cremer, *J. Am. Chem. Soc.*, 2006, **128**, 7168–7169.
18 C. Jeppesen, J. Y. Wong, T. L. Kuhl, J. N. Israelachvili, N. Mullah, S. Zalipsky and C. M. Marques, *Science*, 2001, **293**, 465–468.
19 S. Daniel, A. J. Diaz, K. M. Martinez, B. J. Bench, F. Albertorio and P. S. Cremer, *J. Am. Chem. Soc.*, 2007, **129**, 8072–8073.
20 L. Kam and S. G. Boxer, *Langmuir*, 2003, **19**, 1624–1631.
21 R. J. White, B. Zhang, S. Daniel, J. M. Tang, E. N. Ervin, P. S. Cremer and H. S. White, *Langmuir*, 2006, **22**, 10777–10783.
22 L.-F. Zhang and S. Granick, *Proc. Natl. Acad. Sci. U. S. A.*, 2005, **102**, 9118–9121.
23 M. A. Deverall, S. Garg, K. Ludtke, R. Jordan, J. Ruhe and C. A. Naumann, *Soft Matter*, 2008, **4**, 1899–1908.
24 M. A. Deverall, E. Gindl, E. K. Sinner, H. Besir, J. Ruehe, M. J. Saxton and C. A. Naumann, *Biophys. J.*, 2005, **88**, 1875–1886.
25 R. J. Hill, *Phys. Rev. E: Stat., Nonlinear, Soft Matter Phys.*, 2004, **70**, 051406–051415.
26 W. B. Russel, D. A. Saville and W. R. Schowalter, *Colloidal dispersions*, Cambridge University Press, New York, 1989.
27 H.-Y. Zhang and R. Hill, *J. R. Soc. Interface*, 2010.
28 S. R. Chary and R. K. Jain, *Proc. Natl. Acad. Sci. U. S. A.*, 1989, **86**, 5385–5389.
29 S. Seiffert and W. Oppermann, *J. Microsc.*, 2005, **220**, 20–30.